Supporting Information

Two-dimensional microporous GAM-6 formed by the interzeolite conversion of CoAPO-5

Kenichi Komura,*[a] Edo, Imai,[a] Kazuma Oka,[a] and Takuji Ikeda *[b]

[a] *Department of Materials Science and Processing, Graduated School of Natural Science and Technology, Gifu University, Yanagido 1-1, Gifu 501-1193, Japan.*
[b] *National Institute of Advanced Industrial Science and Technology (AIST), 4-2-1 Nigatake, Sendai 983-8551, Japan.*

EXPERIMENTAL

Characterizations

Powder X-ray diffraction (XRD) diagrams (Shimadzu XRD-6000) were measured using Cu Kα radiation (λ = 1.5418 Å). Elemental analysis was performed using X-ray fluorescence spectroscopy (XRF; Bruker S8 TIGER). Ammonia temperature-programmed desorption (NH_3-TPD) experiments were conducted on a TPD-66 apparatus (Bel Japan): the sample was evacuated at 400 °C for 1 h, and ammonia was adsorbed at 100 °C followed by further evacuation for 1 h. Then, the sample was heated from 100 °C to 710 °C at a temperature increase of 10°C/min in a helium stream. Thermogravimetric (TGA) and differential thermal analysis (DTA) were conducted using an apparatus (Shimadzu DTG-50) with a ramp rate of 10 °C/min under an air stream. The crystal size and morphology were measured using field-emission scanning electron microscopy (FE-SEM) (S-4800; Hitachi High-Technologies, Japan). UV-vis measurement was used with a Lambda 950 UV/VIS/NIR Spectrometer (Perkin Elmer, Inc.). Nitrogen adsorption isotherm measurements were performed using an absorption analyzer (Bel Japan Belsorp 28SA). Priory to measure, the sample is degassed by treatment at 100 °C for 1 h and then for 4 h at room temperature in vacuo.

Solid-state ^{31}P and ^{27}Al magic angle spinning (MAS) nuclear magnetic resonance (NMR) and ^{31}P MAS NMR spectra were recorded, and 1D and 2D solid-state MAS NMR measurements took place using an AVANCEIII 400WB spectrometer (Bruker Biospin K.K., Japan) with a 3.2 mm VT-MAS probe. ^{27}Al 3QMAS NMR spectrum with z-filter was also measured with {^{1}H} decoupling and rotor spinning rate of 24 kHz. {^{1}H}-^{13}C CP/MAS spectrum for as-synthesized GAM-6 was collected at 100.62 MHz with a spinning rate of 6 kHz for ^{13}C. $(NH_4)_2HPO_4$ powder, 1.0 M $AlCl_3$ aqueous solution, adamantane powder, and distilled water were used as chemical shift secondary reference materials for ^{31}P, ^{27}Al, ^{13}C, and ^{1}H nuclei.

Preparation of the parent CoAPO-5

The parent CoAPO-5 zeolite was prepared according to the modified procedure as follows [S1]; The

dissolved solution of $Al(O^iPr)_3$ (10.2 g, 25 mmol) in distilled water (41 g) was added the mixed solution of H_3PO_4 (85 wt%, 7.5 g, 32.5 mmol) and $Co(OAc)_2 \cdot 4H_2O$ (0.623 g, 2.5 mmol) at ambient temperature. The resulting mixture was stirred for 1 h, and then, triethylamine (TEA) (3.28 g, 32.5 mmol) was added. After stirring for 2 h at room temperature, the resulting gel (mol ratio; Al_2O_3 : P_2O_5 : CoO : TEA : H_2O = 1.0 : 1.3 : 0.1 : 1.3 : 150) was transferred to Teflon-lined autoclave and stood at 170 °C for 6 h. After cooling down, the formed solid was filtrated, washed with distilled water, and dried at 90 °C for overnight to obtain as-synthesized CoAPO-5. To remove the containing TEA, the calcination was taken place at 550 °C (ramping rate = 1 °C/min.) for 6 h to obtain the calcined CoAPO-5 zeolite.

[S1] W. Yang, W. Sun, S. Zhao and X. Yin, *Micropor. Mesopor. Mater.*, 2016, **219**, 87.

The interzeolite conversion (*izc*MAP) of CoAPO-5 to GAM-6

In a polypropylene (PP) cup, the resolved solution of a prescribed amount of piperidine (0.837 g, 9.84 mmol) in distilled water (4.05 g) was added to the calcined CoAPO-5 zeolite (1.0 g). The resulting suspension (molar ratio, T_2O_x ($3 < x < 5$) : OSDA : H_2O = 1.0 : 1.2 : 27.5) was stirred for 1 h, and transferred to a Teflon-lined autoclave. The *izc*MAP was carried out at 170 °C for 5 days. After cooling to ambient temperature, the formed product was filtrated, washed with distilled water, and dried at 90 °C to obtain the as-synthesized GAM-6 crystal. The calcination was taken place at 350 °C (ramping rate = 0.5 °C/min.) for 24 h to obtain open-framework GAM-6.

Catalytic cracking reactions of olefins

Cracking reactions were taken place according to our reported procedure as follows [S2]; the calcined GAM-6 (20 mg, 18–32 mesh) was installed onto a glass wool fixed in a quartz tube (diameter 3.4 mm, length 100 mm) connecting with gas chromatography (Shimadzu GC-14A, capillary column: Ultra-1, 30 m x 0.53 mm). Reactions were performed by adding a 0.04 mL of substrate (1-hexene and 2-methyl-1-heptene) at 300 °C under nitrogen flow (40 mL/min), and the catalytic activity was evaluated by their conversions.

[S2] H. Suzuoki, S. Takegawa and K. Komura, *J. Jpn. Petrol. Inst.*, 2014, **57**, 184.

Structure analysis

To efficiently determine the framework structure of GAM-6, the structural analysis was carried out on a calcined sample excluding OSDA. High-resolution X-ray powder diffraction data were collected on the Bruker D8-advance instrument with modified Debye-Scherrer optics at room temperature. A wavelength of Cu $K\alpha_1$ was used, and the output was 40 kV–50 mA. A powder sample was packed into a borosilicate glass capillary tube with an inner diameter of 0.5 mmϕ. Background levels across all measured 2θ ranges were very high due to fluorescent X-rays from the Co atoms in the sample.

The most probable lattice constants and space group of calcined GAM-6 were estimated by the

indexing program conograph [S3]. A hexagonal system (space group $P6_3$, $P6_3/m$, or $P6_322$) was derived. As a result, the space group $P6_322$ was the correct solution. The initial integral intensities of each reflection $|F_{obs}|$ were extracted from obtained powder XRD data by the Le Bail method. The initial structure model was successfully solved by the powder charge flipping (pCF) method from 439 $|F_{obs}|$ data ($d < 1.0$ Å) using the program Superflip [S4]. The framework structure of GAM-6 is constructed by two tetrahedral Al sites, two octahedral Al sites, one tetrahedral P site, and seven O sites, corresponding to all constituent atoms of the framework (Figure 2 and S13).

Obtained structural data were refined by the Rietveld method using the program RIETAN-FP [S5]. The crystal structure was visualized using the programs VESTA3 [S6] and CrystalMaker (CrystalMaker Software Limited, England). During the structure refinement of GAM-6, we imposed restraints upon all the Al–O and P–O bond lengths and all the O–Al–O and O–P–O bond angles. For sites with the same elements, the isotropic atomic displacement parameter, B, was constrained equally using linear constraints, and the same constraints were adopted for individual element sites. Sufficiently small R factors indicate that the final structural model reasonably explains the other experimental results. Finally, observed, calculated, and difference patterns resulting from Rietveld analysis are shown in Figure S14. Next, we describe the analytical procedure in more detail.

It was assumed that the Co atom is substituted for Al sites. Al/P and (Al+Co)/P ratios were calculated to be 1.45 and 1.59, respectively, by the EDX elemental analysis. No elements other than Al, P, Co, O, and C were detected in this analysis. This finding indicated dealumination in the framework considering the number of T atoms in the framework structure obtained.

From the result of the UV-visible spectrum (Figure S8), Co^{II} and Co^{III} ions are likely to coexist, and a Co atom could be substituted for both four- and six-coordinated Al atoms. (The conclusion is that it was difficult to distinguish between Co and Al in the Rietveld analysis.) Therefore, all Al sites were treated as solid solution sites in this analysis with a ratio of Co : Al = 0.0847 : 0.9153 applied according to the result of the EDX analysis. When the occupancy parameters were refined, g(Al1) and g(Al4), became less than 1.0, suggesting the presence of Al atom vacancy at two octahedral Al sites. Then, careful refinement of g(Al) applied constraints to satisfy Al/P = 1.45 obtained from EDX analysis resulted in a convergence of g(Al1) = 0.8194 and g(Al4) = 0.6911, respectively (Table S3).

The framework composition without Al atom vacancy was calculated as $(Al(Co))_{20}P_{12}O_{68}$. This composition will be negatively charged, which is inappropriate as is. Therefore, some H^+ ions (or counter-cations) for charge compensation should be included in the framework. In the model where defects in Al atoms are present, further refinement of oxygen sites showed that the occupancy of site O6 located between sites Al3 and Al4 increased to ca. 1.2, whereas those of the other O sites were close to or below 1.0. Therefore, we assume that H is attached to site O6. The value of g(O6) was corrected by multiplying by 1.125 (=7/6) for convenience, including the scattering amplitude of H atoms.

As described above, Al atom vacancy may occur at sites Al1 and Al4. In that case, oxygen atoms adjacent to the two Al sites should have a proton associated with them. The site O6 that corresponds

to site Al4 is already treated as OH. Then, the site O2 adjacent to the vacancy part of site Al1 was considered the –OH group, and the constraint of g(O2) = g(Al1)+1.125×(1–g(Al1)) = 1.125–0.125×g(Al1) was applied.

In addition, we examined whether H^+ is present in the ring center of the framework structure, as in the distribution of alkali metal cations common in aluminosilicate zeolites. The H atom was fixed at the gravity center of 3, 4, 5, or 6-rings in the framework structure, and only the g(H) values were refined. Then, the presence of an H atom was strongly suggested near the center of the 3-ring composed of Al3-Al3-Al4 (site H1), and a localized electron density was observed by the maximum-entropy method. The H1 position corresponds to the 6*h* (x, 2x, 1/4) site. However, the site H1 is not included in the structural model because the refinement of a single hydrogen atom would be an overestimation based on the inadequate precision of this data. The exact location of the H atom is difficult to determine at this time and will be investigated further.

The above consideration leads to the framework composition, including the H^+ cation for charge compensation, was estimated to be $H_{4.8}Co_{1.6}Al_{17.4}P_{12}O_{53.8}(OH)_{14.2}$.

Five adsorbed water molecule (WO*n*) sites were found in the 2D micropore. About each WO site, the interatomic distances between WO–WO and between the framework atom and WO are more than 2 Å apart. Among them, the WO2 site was located near the Al3 site and appeared to form a five-coordinated AlO_5. Site WO5 is located at the center of 6-ring composed of three P1 and three Al3 atoms viewed along the *c*-axis. It is noted that a part of WO may be a residual hydrocarbon species since the calcination temperature was somewhat lower than the combustion temperature of OSDA. However, a large volume electron density derived from piperidine was not observed in micropores. The crystallinity of GAM-6 was slightly degraded by calcination as shown in Figure 2, and some amorphous fractions containing residual hydrocarbon species may coexist in the sample.

Figure S15 shows the elucidated structure of the calcined GAM-6 viewed along (a) [110] and (b) [100] directions. (Black-box line indicates unit cell. Purple stands for P atom, red for Al, light green for O, flesh color for H atom, and sky-blue for H_2O. The pie chart for each atom represents the site occupancy for them. In addition, obtained crystallographic information is summarized in Table S2. A crystallographic information file (CIF) was disclosed in Table S3. Selected atom distances and angles are listed in Table S4. The validity of the interatomic distances of the framework was confirmed by the bond valence sum rule [S7], where the bond valence parameters R_0 of 1.651 and 1.617 [S8] were applied for Al^{3+}–O^{2-} bond and P^{5+}–O^{2-} bond, respectively, and the empirical constant of 0.37 was applied. The bond valence sums and the effective coordination numbers of each Al and P site were disclosed in Table S4. Calculated values are reasonable. The values obtained are within the permissible range, meaning the average interatomic distances are also reasonable.

[S3] R. Oishi-Tomiyasu, *Acta Cryst.*, 2016, **A72**, 73.
[S4] L. Palatinus and G. Chapuis, *J. Appl. Cryst.*, 2007, **40**, 786.
[S5] F. Izumi and K. Momma, *Solid State Phenom.*, 2007, **130**, 15.
[S6] K. Momma and F. Izumi, *J. Appl. Crystallogr.*, 2011, **44**, 1272.

[S7] D. Altermatt and I. D. Brown, *Acta Crystallogr.*, 1985, **B41**, 244.
[S8] https://www.iucr.org/resources/data/data-sets/bond-valence-parameters

Contents

Tables

Figures

Table S1. Textural parameters of the parent zeolite CoAPO-5 and the child GAM-6.

sample	composition [d] (mol ratio)				surface area [e]	pore volume [e]
	Al/P	Co/Al	Co/P	(Co + Al) / P	$m^2\ g^{-1}$	$mL\ g^{-1}$
CoAPO-5 [a]	0.733	0.495	0.363	1.097	356	0.23
GAM-6 [b]	1.451	0.0925	0.134	1.585	237	0.20
GAM-6 [c]	1.45	0.093	0.134	1.59	—	—

a. Used parent zeolite in this study, of its Co content is 0.10 (Co + Al) / P.
b. Calcined GAM-6.
c. The elucidated structure of GAM-6 by the Rietveld refinement.
d. Chemical compositions. (Measured by XRF for CoAPO-5 and by EDX for GAM-6 [b]. Estimated from structure model)
e. Estimated from N_2 adsorption isotherm.

Table S2. Experimental conditions and crystallographic information.

Compound name	calcined GAM-6
Refined chemical composition	$\lvert(H_2O)_{32.2}\rvert\cdot[Co_{1.6}Al_{17.4}P_{12}O_{56}(OH)_{14.2}]$
Estimated chemical composition	$\lvert H_{4.8}\,(H_2O)_{32.2}\rvert\cdot[Co_{1.6}Al_{17.4}P_{12}O_{56}(OH)_{14.2}]$
Space group	$P6_322$
a / nm	0.945482(9)
c / nm	2.34504(4)
Unit-cell volume / nm^3	1.81546(4)
2θ range / °	5.5–110.1
Step size (2θ) / °	0.016346
Profile range in FWHM	12
Number of observations	6442
Number of contributing reflections	526
Number of refined structural parameters	45
Number of constraints	37
R-factors obtained by Rietveld analysis	
R_{wp}	0.018
R_p	0.014
R_F	0.040
R_{Bragg}	0.043
R_{exp}	0.008
χ^2	5.72

Table S3. A crystallographic information files (CIF) of the calcined GAM-6.

```
#======================================================================
data_VESTA_phase_1

_chemical_name_common                  'calcined GAM-6'
_cell_length_a                         9.45484(9)
_cell_length_b                         9.45484(9)
_cell_length_c                         23.4504(4)
_cell_angle_alpha                      90.000000
_cell_angle_beta                       90.000000
_cell_angle_gamma                      120.000000
_cell_volume                           1815.47(4)
_space_group_name_H-M_alt              'P 63 2 2'
_space_group_IT_number                 182

loop_
_space_group_symop_operation_xyz
   'x, y, z'
   '-y, x-y, z'
   '-x+y, -x, z'
   '-x, -y, z+1/2'
   'y, -x+y, z+1/2'
   'x-y, x, z+1/2'
   'y, x, -z'
   'x-y, -y, -z'
   '-x, -x+y, -z'
   '-y, -x, -z+1/2'
   '-x+y, y, -z+1/2'
   'x, x-y, -z+1/2'

loop_
   _atom_site_label
   _atom_site_fract_x
   _atom_site_fract_y
   _atom_site_fract_z
   _atom_site_occupancy
   _atom_site_symmetry_multiplicity
   _atom_site_Wyckoff_symbol
   _atom_site_adp_type
   _atom_site_U_iso_or_equiv
   _atom_site_type_symbol
Al1    0           0           0.25          0.82(9)     2 b Uiso    0.0467(12)    Al
Al2    0           0           0.0712(3)     1           4 e Uiso    0.0467(12)    Al
Al3    0.4695(6)   0.0159(8)   0.3114(3)     1          12 i Uiso    0.0467(12)    Al
Al4    0.33333     0.66667     0.25          0.69(9)     2 c Uiso    0.0467(12)    Al
P1     0.2825(6)   0.0815(6)   0.1529(2)     1          12 i Uiso    0.0467(12)    P
O1     0.5522(9)   0.1044(9)   0.25          1           6 h Uiso    0.034(2)      O
O2     0.0148(10)  0.1723(7)   0.2053(3)     1.0226     12 i Uiso    0.034(2)      O
O3     0.3567(11)  0.2701(14)  0.1588(4)     1          12 i Uiso    0.034(2)      O
O4     0.4103(14)  0.0251(14)  0.1463(4)     1          12 i Uiso    0.034(2)      O
O5     0.1900(9)   0.0506(11)  0.0924(5)     1          12 i Uiso    0.034(2)      O
O6     0.172(1)    0.505(1)    0.2926(5)     1.125      12 i Uiso    0.034(2)      O
O7     0           0           0             1           2 a Uiso    0.034(2)      O
WO1    0.289(3)    0.912(2)    0.5316(9)     1          12 i Uiso    0.380(12)     WO
WO2    0.328(3)    0.442(2)    0.1129(13)    0.70(2)    12 i Uiso    0.380(12)     WO
WO3    0.421(4)    0.848(3)    0.478(2)      0.59(2)     2 i Uiso    0.380(12)     WO
WO4    0.33333     0.66666     0.576(3)      0.64(2)     4 f Uiso    0.380(12)     WO
WO5    0.66667     0.33333     0.301(2)      0.54(3)     4 f Uiso    0.380(12)     WO
#======================================================================
```

Table S4. Selected atomic distances, d / Å, angles, ϕ / (°) for the calcined GAM-6, and calculated bond valence sum (BVS) and effective coordination number (ECN) of each Al and P atom.

d	(Å)
Al1 – O2	1.886(5) × 6
Average	1.883
Al2 – O5	1.687(7) × 3
Al2 – O7	1.666(6)
Average	1.682
Al3 – O6	1.644(7)
Al3 – O1	1.652(7)
Al3 – O4	1.661(10)
Al3 – O3	1.669(11)
Average	1.644
Al4 – O6	1.819(5) × 6
Average	1.819
P1 – O4	1.553(10)
P1 – O3	1.563(10)
P1 – O4	1.615(10)
P1 – O5	1.627(7)
Average	1.590

ϕ	(°)
O2 – Al1 – O1	83.2(4) × 3
O2 – Al1 – O2	91.7(3) × 6
O2 – Al1 – O2	93.7(5) × 3
O2 – Al1 – O2	172.6(5) × 3
O7 – Al2 – O5	107.3(5) × 3
O5 – Al2 – O5	111.6(5) × 3
Average	109.45
O6 – Al3 – O1	102.4(7)
O6 – Al3 – O4	113.9(7)
O6 – Al3 – O3	103.7(5)
O1 – Al3 – O4	108.9(4)
O1 – Al3 – O3	113.4(5)
O4 – Al3 – O3	114.0(6)
Average	109.38
O6 – Al4 – O6	86.3(5) × 3
O6 – Al4 – O6	85.7(6) × 3
O6 – Al4 – O6	94.0(4) × 6
O6 – Al4 – O6	179.6(4) × 3
O4 – P1 – O3	114.7(7)
O4 – P1 – O5	107.1(5)
O4 – P1 – O2	110.8(6)
O3 – P1 – O5	100.3(6)
O3 – P1 – O2	111.0(5)
O5 – P1 – O2	112.5(5)

Site	BVS	ECN
Al1	2.605	6.00
Al2	3.679	4.00
Al3	3.941	4.00
Al4	2.634	6.00
P1	4.327	3.94

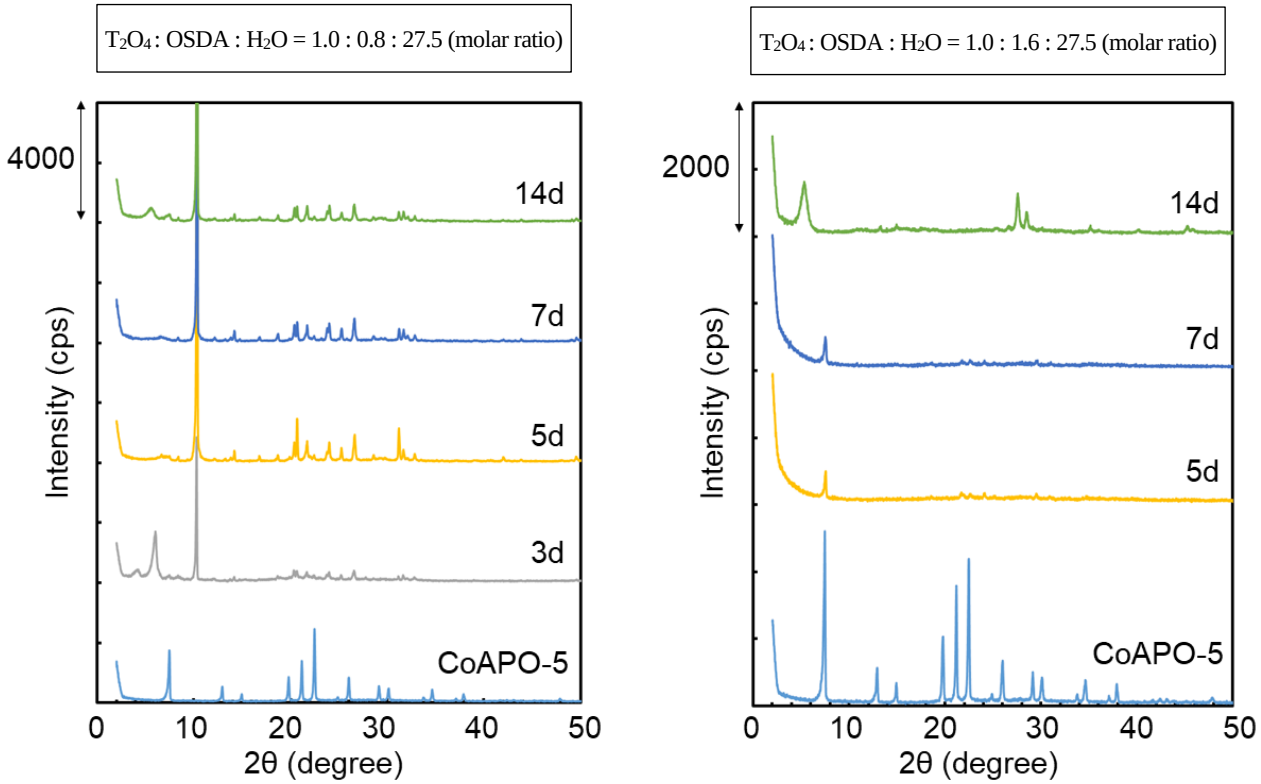

Fig. S1. Powder XRD charts of the parent CoAPO-5 and the obtained samples under different conditions.

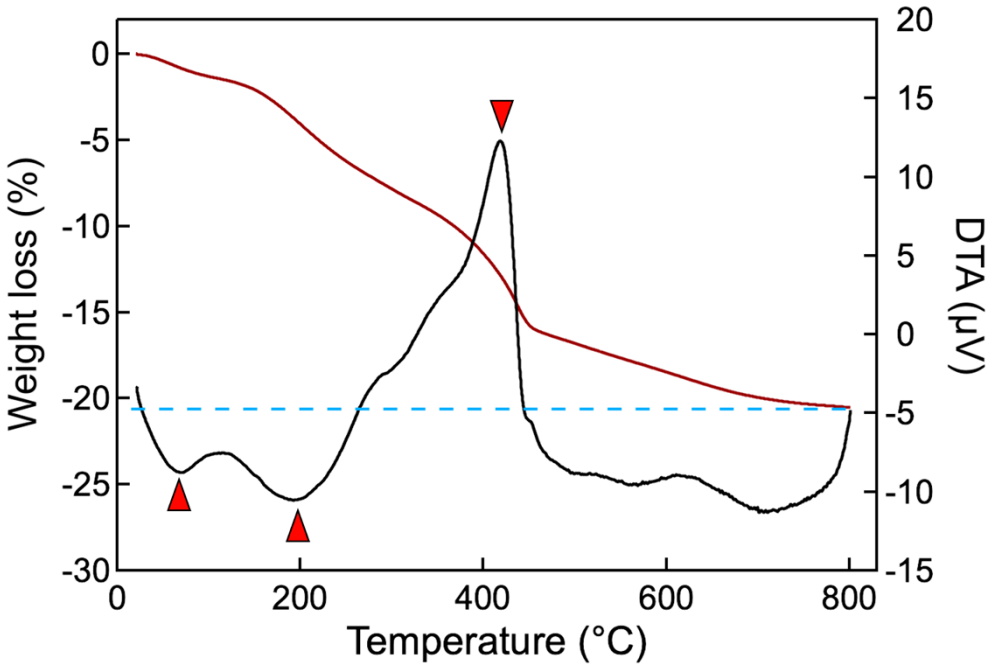

Fig. S2. TG-DTA charts of the as-synthesized GAM-6.

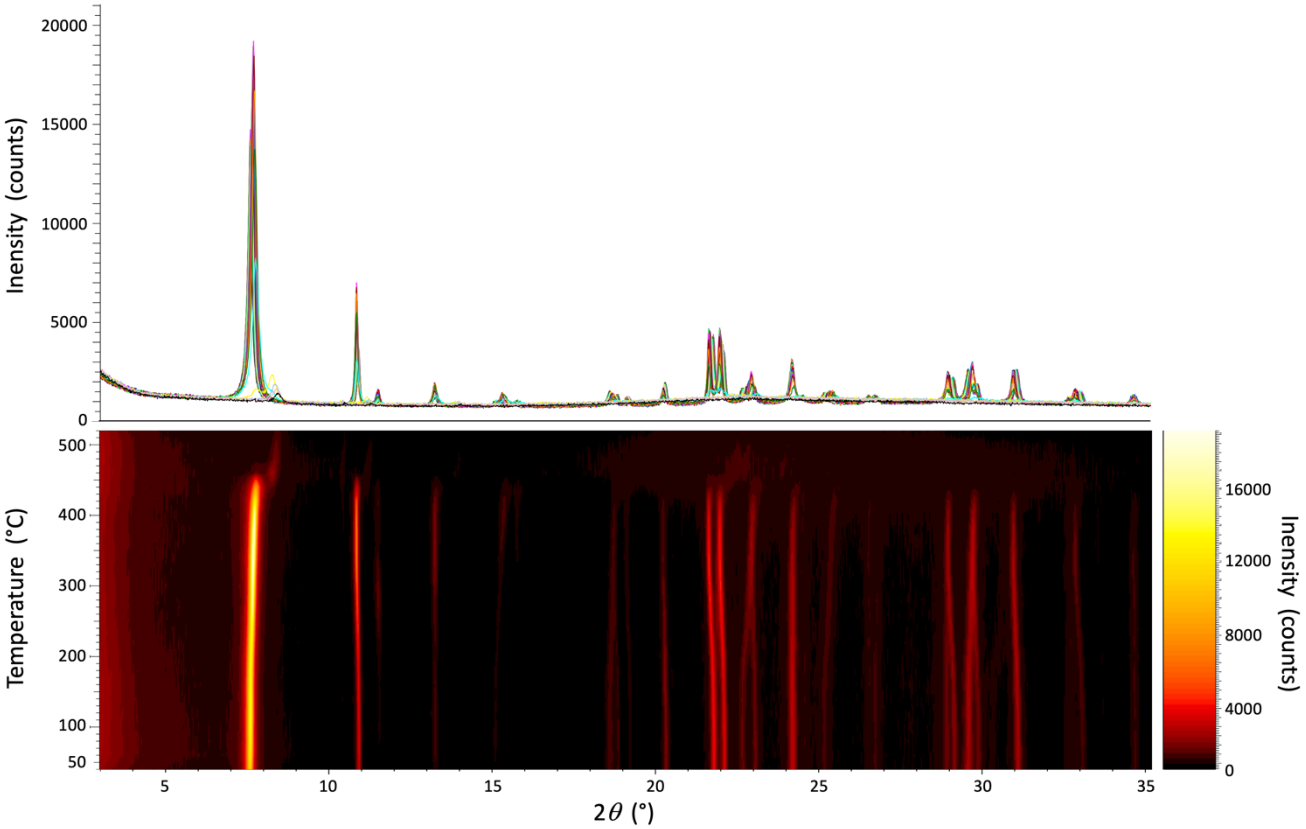

Fig. S3. HT-XRD 2D diagrams of the GAM-6.

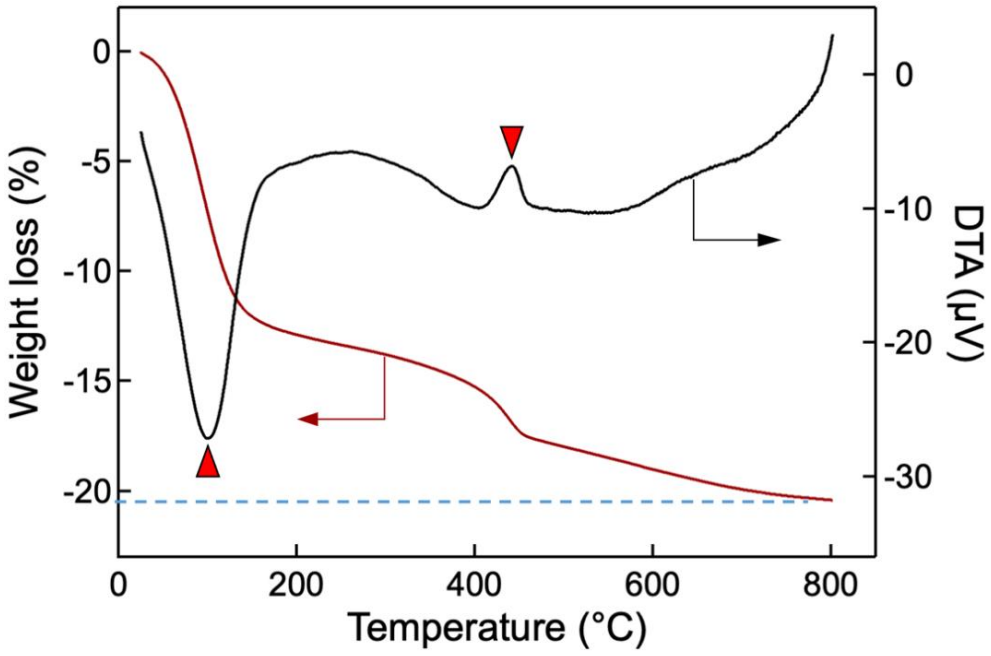

Fig. S4. TG-DTA chart of the calcined GAM-6.

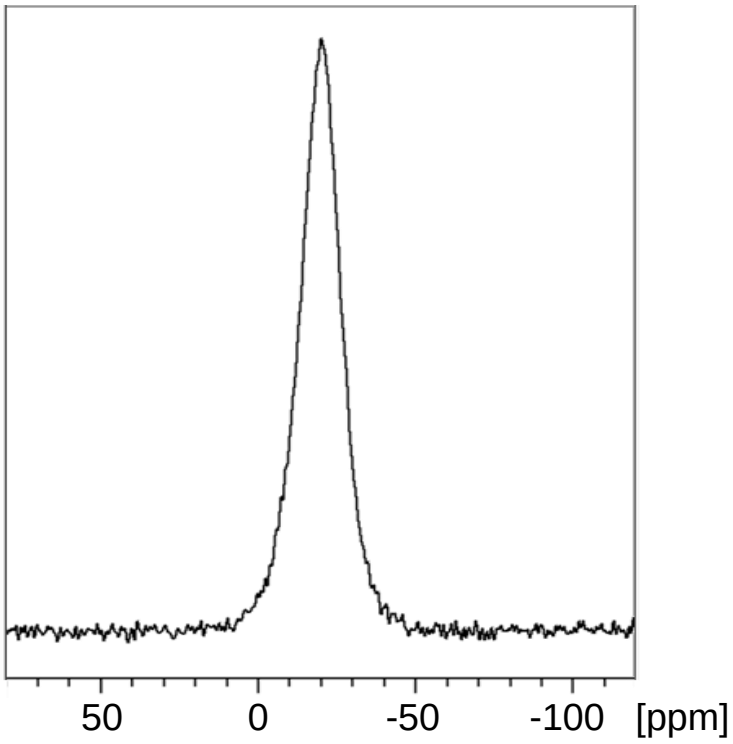

Fig. S5. ^{31}P DPMAS NMR spectrum of the calcined GAM-6.

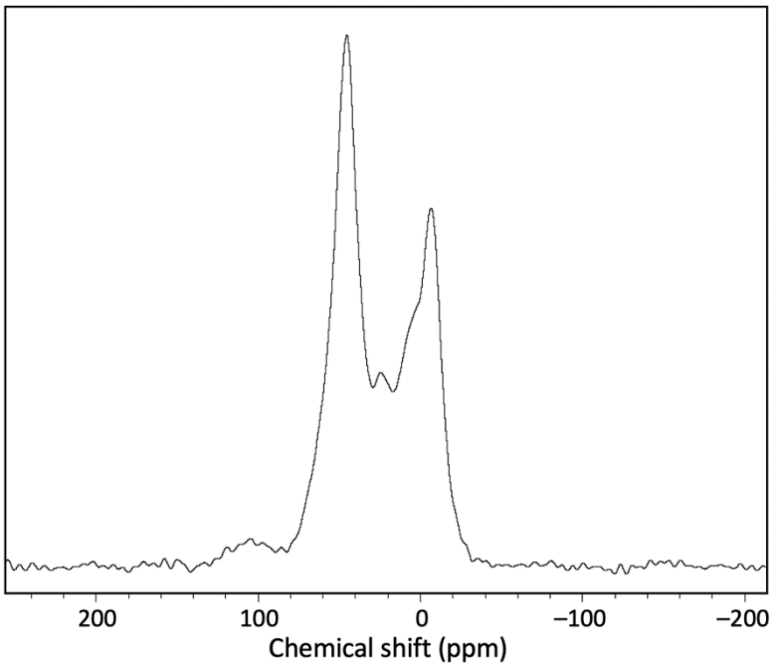

Fig. S6. ^{27}Al MAS NMR spectrum of the calcined GAM-6.

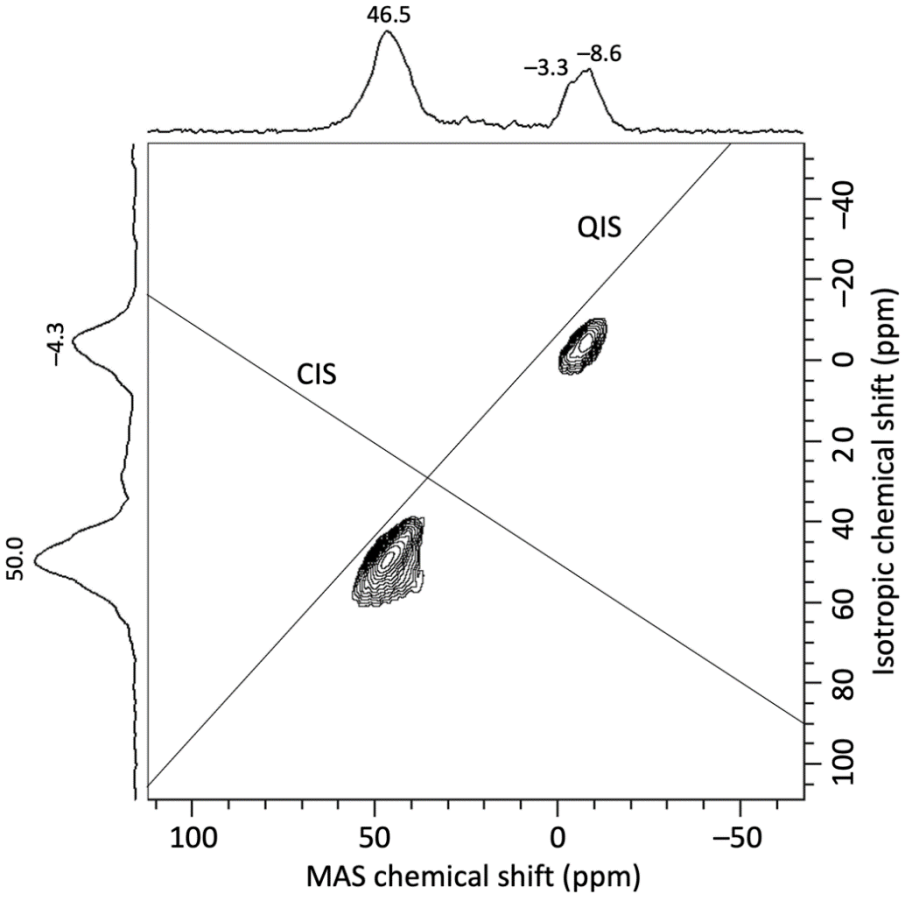

Fig. S7. ^{27}Al 3QMAS NMR spectrum of the calcined GAM-6.

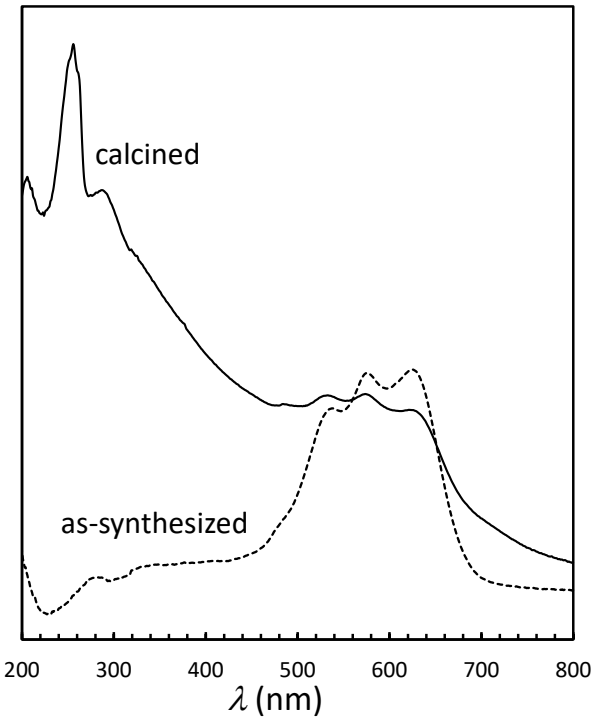

Fig. S8. UV-visible chart of the as-synthesized, and the calcined GAM-6.

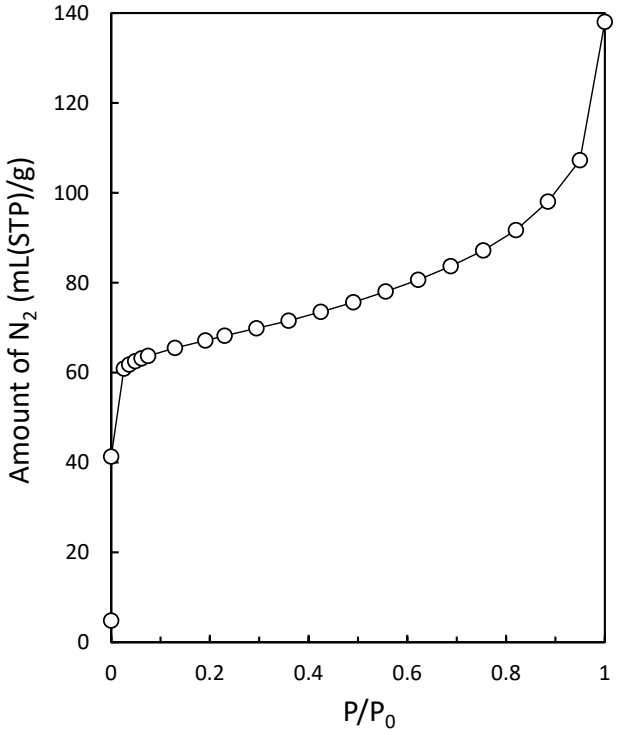

Fig. S9. Nitrogen adsorption isotherm of the calcined GAM-6.

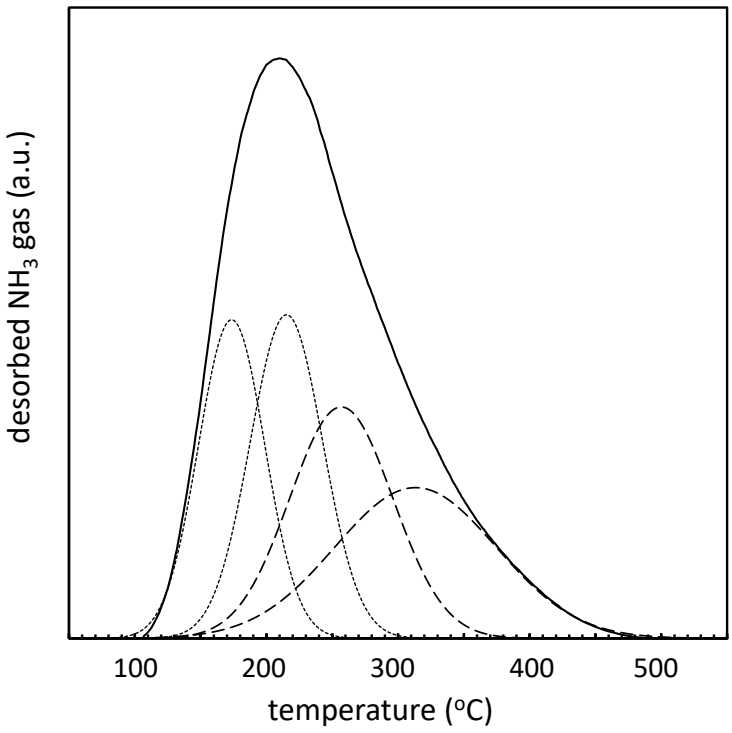

Fig. S10. NH_3-TPD chart of the calcined GAM-6.

Additional Note: The framework density (FD) of GAM-6 is calculated to be about 17.6 from the ideal framework structure. It can be seen that the nitrogen up-take seems to be small relative to the GAM-6 structure (Fig. S9). The specific surface area obtained from gas adsorption measurements may be small compared to other zeolites with 10-ring 2D pores. This can be attributed to the increase in amorphous components, as the crystallinity of GAM-6 decreases during the calcination process. In other words, the specific surface area may be smaller than it appears. It is also possible that pore blockage may have partially occurred in association with the decrease in crystallinity and with trace amounts of remaining OSDA. Of course, these influence may cause an inaccurate value of the Brønsted site by NH_3-TPD analysis. However, it is generally known that these values of which material prepared via calcination process are relied on the sample rather than those estimated by the framework structure. Consequently, it is obvious that the estimated surface area (237 m^2/g) and the quantity (0.532 mmol/g) of GAM-6 are reasonable values compared with those of reported AlPOs and metal-AlPOs [S9-S12].

[S9] D. B. Akolekar, *Zeolites*, 1996, **17**, 283.
[S10]Z. Wang, Z. Tian, F. Teng, G. Wen, Y. Xu, Z. Xu, L. Lin, *Catal. Lett.*, 2005, **103**, 109.
[S11]I. A. Tiuliukova, N. A. Rudina, A. I. Lysikov, S. V. Cherepanova, E. V. Parkhomchuk, *Mater. Lett.*, 2018, **228**, 61.
[S12] S. Tao, Z. Wang, L. Wang, X. Li, Y. Wang, B. Wang, W. Zi, Y. Wei, K. Chen, Z. Tian, G. Hou, *J. Am. Chem. Soc.*, 2023, **145**, 4860.

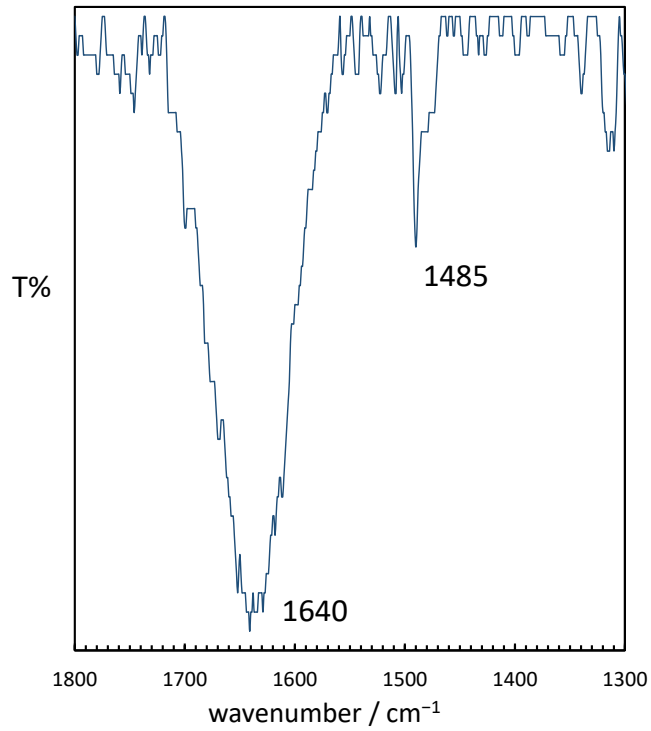

Fig. S11. FTIR spectrum of pyridine adsorbed GAM-6 at room temperature (Expanded at 1300-1800 cm^{-1} region).

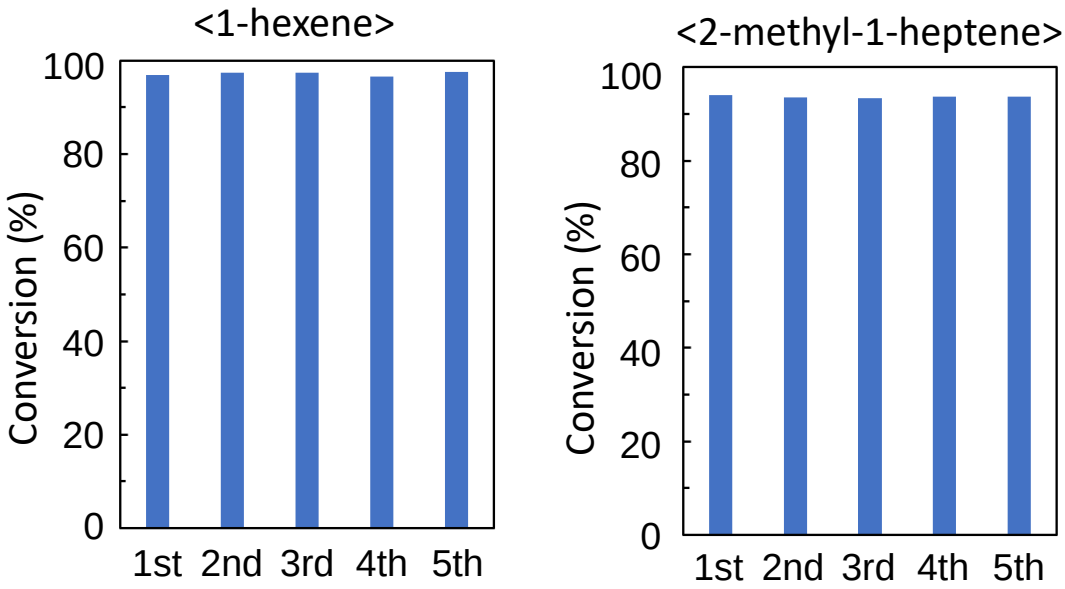

Fig. S12. Results of catalytic cracking reactions over GAM-6.

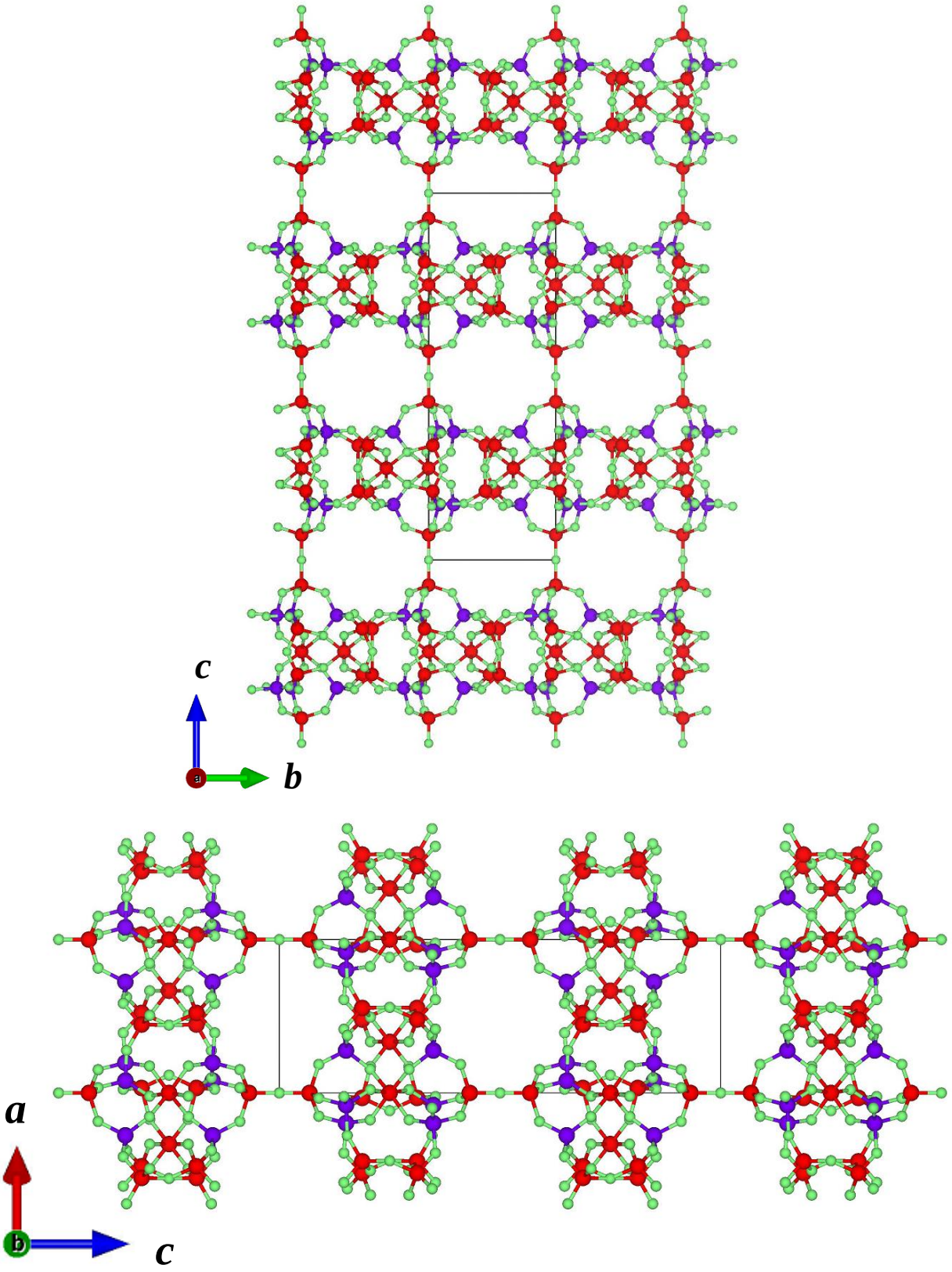

Fig. S13. The framework structure of the calcined GAM-6 viewed along the *a*-axis (up) and the *b*-axis (down).

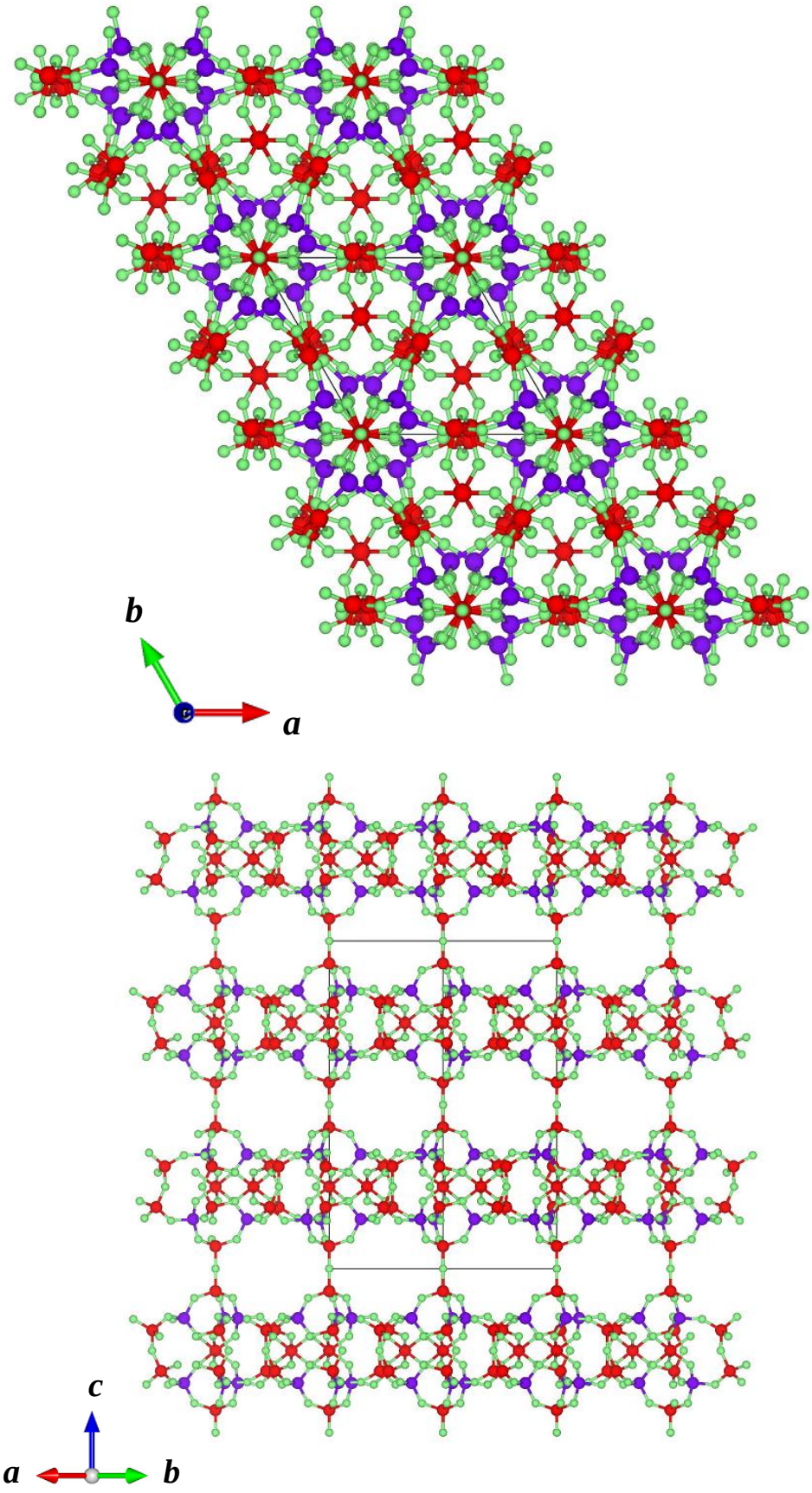

Fig. S13. (Continued) The structure of the calcined GAM-6 viewed along the *c*-axis (up) and the [110] direction (down).

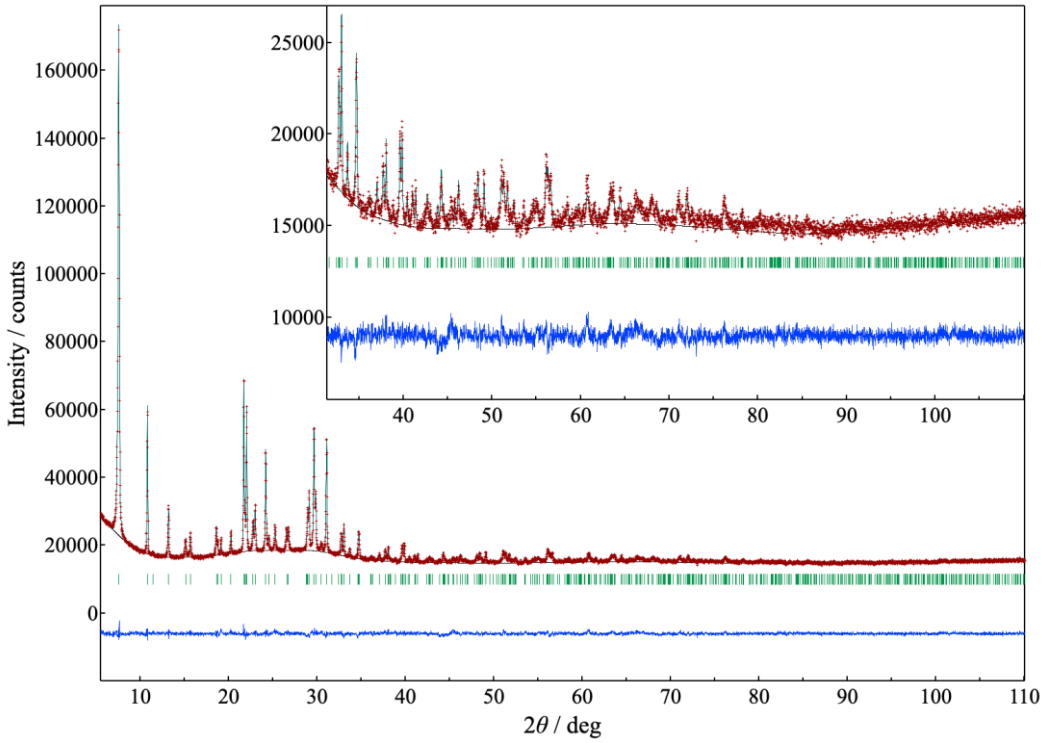

Fig. S14. Observed (red), calculated (dark-blue), and difference (blue) patterns resulting from Rietveld analyses of the calcined GAM-6. Green vertical bars denote positions of Bragg reflections for calcined GAM-6.

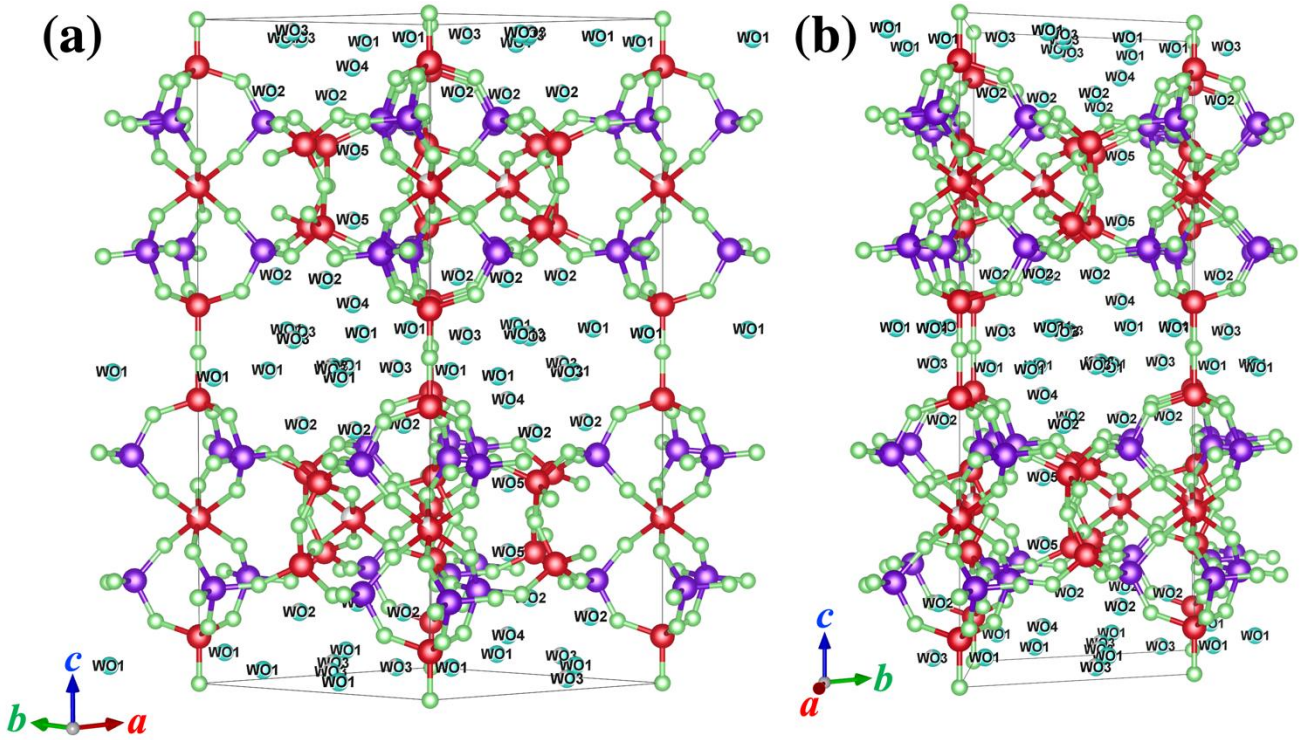

Fig. S15. Refined crystal structure of the calcined GAM-6 viewed along (a) [110] and (b) [100] directions.